Supporting Information

Titanium Compounds Containing Naturally Occurring Dye Molecules

Wei-Hui Fang,* Rosa Müller, Rajesh B. Jethwa, Victor Riesgo-González, Ning Li, Sebastian D. Pike, Andrew D. Bond, He-Kuan Luo, Cheng Zhang, Dominic S. Wright*

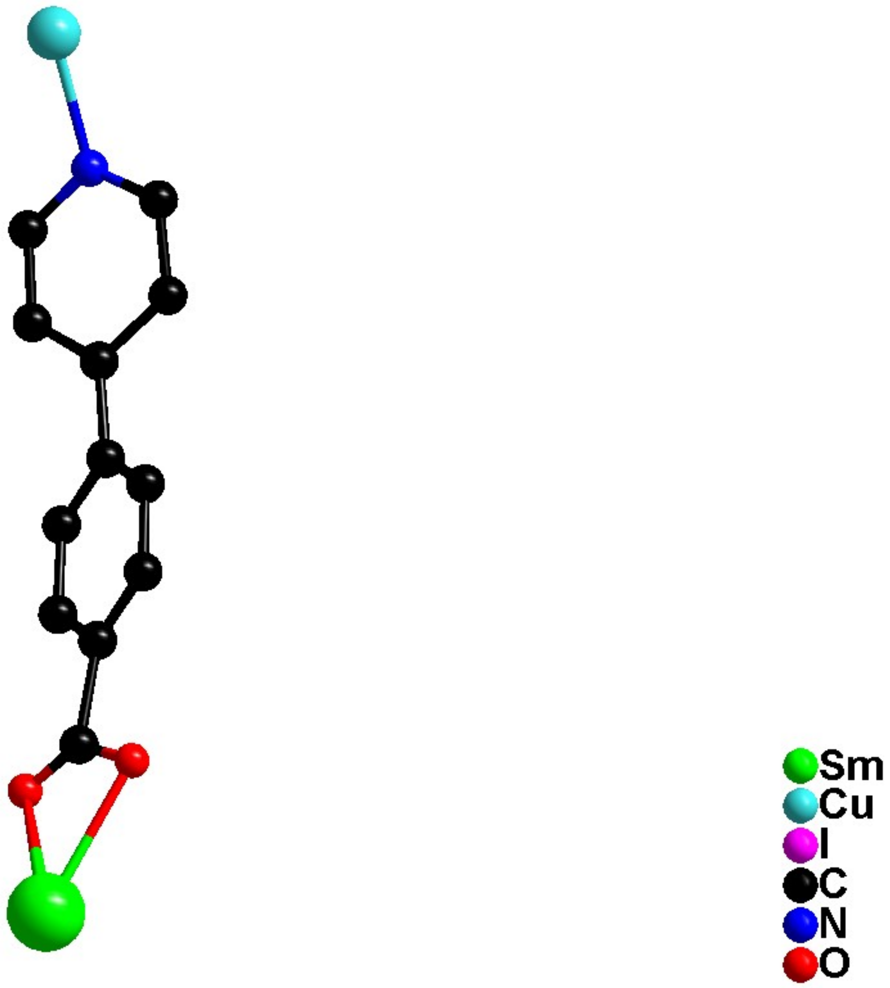

1. General Experimental Section

Materials and physical measurements. All chemicals were purchased from commercial companies (Sigma-Aldrich and Fisher Scientific) and used as received. Strict inert-atmospheric conditions (dry and O_2-free) were employed throughout all synthetic and handling procedures [i.e., vacuum-line and using a glove-box (Saffron type α)]. Elemental analysis was performed using a PerkinElmer 240 Elemental Analyser. Infrared (IR) spectroscopic measurements were performed on powdered samples using a Perkin-Elmer Spectrum One FT-IR setup fitted with a diamond attenuated total reflectance system. UV-Vis diffuse reflectance spectra were recorded using a VARIAN Cary 50 Bio UV-Visible Spectrophotometer. TGA data were acquired on a Mettler Toledo TGA/DSC. NMR spectroscopy was carried out on a Bruker AV-500 instrument using d^8-toluene solvent, all chemical shifts are reported in parts per million.

General Methods for X-ray Crystallography. X-ray crystallographic data were collected using a Bruker D8-QUEST PHOTON-100 diffractometer equipped with an Incoatec IμS Cu microsource (Cu Kα, λ= 1.5418 Å). The temperature was held at 180(2) K using an Oxford Cryosystems N_2 cryostat. Data integration and reduction were undertaken with SAINT in the APEX3 software suite. Multi-scan corrections were applied using SADABS. Structures were solved using SHELXT [G.M.Sheldrick, *Acta Cryst.* 2015, A**71**, 3-8] and refined using SHELXL [G.M.Sheldrick, *Acta Cryst.* 2015, C**71**, 3-8].

Cyclic Voltammetry: Electrochemical measurements were performed on an Ivium CompactStat (B10045) using an in-house small-volume cyclic voltammetry cell. Polished 3 mm diameter glassy carbon (Biologic A-012744) was used as the working electrode while coiled platinum wire was used as the counter-electrode. For the non-aqueous reference, silver wire was used in addition to an internal standard of ferrocene {0.52 V *vs.* saturated calomel electrode (SCE)} in dichloromethane. [D. D. Bao, B. Millare, W. Xia, B. G. Steyer, A. A. Gerasimenko, A. Ferreira, A. Contreras, V. I. Vullev, *J. Phys. Chem. A* **2009**, 113, 1259-1267.] As an aqueous reference, a Hg/HgO (1M KOH) reference electrode was used {-0.143 (1M NaOH) vs (SCE)} [Table 4.1, pg 75, Zoski, C. G. *Handbook of Electrochemistry* (Elsevier, 2007)].

Re-crystallised tertiary-butyl-ammonium hexafluorophosphate (2.4084 g) and sublimed ferrocene (5.7 mg) were dissolved in DCM (62.17 mL, dry, degassed) under inert atmosphere to make the supporting electrolyte. A sample of this solution alone was tested by cyclic voltammetry to identify the stability window. Quinizarin (3.1 mg) was dissolved in DCM (13 ml, dry, degassed) under inert atmosphere to form an orange analyte (1 mM) solution. A sample of this was tested under cyclic voltammetry.

Quinizarin (7.7 mg) was dissolved in basic aqueous media (1 M KOH, 32.06 ml, degassed) under inert atmosphere to form a purple analyte (1 mM) solution. A sample of this was tested under cyclic voltammetry.

Re-crystallised tertiary-butyl-ammonium hexafluorophosphate (1.29440 g) and sublimed ferrocene (2 mg) were dissolved in DCM (33.41 mL, dry, degassed) under inert atmosphere to make the supporting electrolyte. **1** (41 mg) was dissolved in this supporting electrolyte solution (23.6 mL) to generate the analyte (1 mM) solution. Cyclic voltammetry of **1** was then performed under inert atmosphere with scans beginning by sampling the oxidative processes, i.e. positive potentials first. Cyclic voltammetry was performed at 50, 100 and 500 mVs^{-1}.

2. Synthesis of New Compounds

Synthesis of $Ti_4(Q)_4(O^iPr)_8 \cdot 2HO$*i*Pr (1). Quinizarin (240 mg, 1.0 mmol) was dissolved in dry isopropanol (30 mL) under an inert gas, and $Ti(O^iPr)_4$ (0.3 mL, 1.0 mmol) was added slowly under vigorous stirring. The suspension changed colour from orange to violet during addition of the $Ti(O^iPr)_4$. After standing at room temperature for 3 days, 228 mg (53 % yield) of dark red crystalline **1** was obtained. Elemental analysis (%) calcd for $C_{86}H_{96}O_{26}Ti_4$: C 59.46, H 5.57; found C 60.08, H 5.85.

Synthesis of $Ti_2LnCl_2(A\text{-}H)_2(O$*i*$Pr)_7 \cdot$x HO*i*Pr (A = alizarin; for compounds 2-5, 8 x = 0; for complexes 6-7 x = 1). (2-8). Similar synthesis procedures are employed for compounds **2-8**. Alizarin (120 mg, 0.50 mmol) and $LnCl_3 \cdot xH_2O$ (1mmol) was dissolved in water-free isopropanol (30 mL) under an inert gas, and excess $Ti(O^iPr)_4$ (2.0 mL, 6.9 mmol) was added slowly under vigorous stirring. The suspension color changed from red to purple when adding $Ti(O^iPr)_4$. After standing still at room temperature for 4 days, approximately 0.120 g (40 % yield) of dark red crystalline material was obtained.

Elemental analysis (%) calcd for compound **2** $C_{49}H_{63}Cl_2O_{15}Ti_2Eu$: C 48.61, H 5.24; found C48.68, H 5.29.

Elemental analysis (%) calcd for compound **3** $C_{49}H_{63}Cl_2O_{15}Ti_2Gd$: C 48.40, H 5.22; found C48.58, H 5.76.

Elemental analysis (%) calcd for compound **4** $C_{49}H_{63}Cl_2O_{15}Ti_2Tb$: C 48.33, H 5.21; found C48.76, H 5.45.

Elemental analysis (%) calcd for compound **5** $C_{49}H_{63}Cl_2O_{15}Ti_2Dy$: C 48.19, H 5.20; found C47.50, H 5.20.

Elemental analysis (%) calcd for compound **6** $C_{52}H_{71}Cl_2O_{16}Ti_2Ho$: C 48.33, H 5.21; found C48.45, H 5.36.

Elemental analysis (%) calcd for compound **7** $C_{52}H_{71}Cl_2O_{16}Ti_2Er$: C 48.60, H 5.49; found C48.61, H 5.55.

Elemental analysis (%) calcd for compound **8** $C_{49}H_{63}Cl_2O_{15}Ti_2Yb$: C 47.78, H 5.15; found C47.77, H 5.15.

3. Characterisation of Compounds and Materials

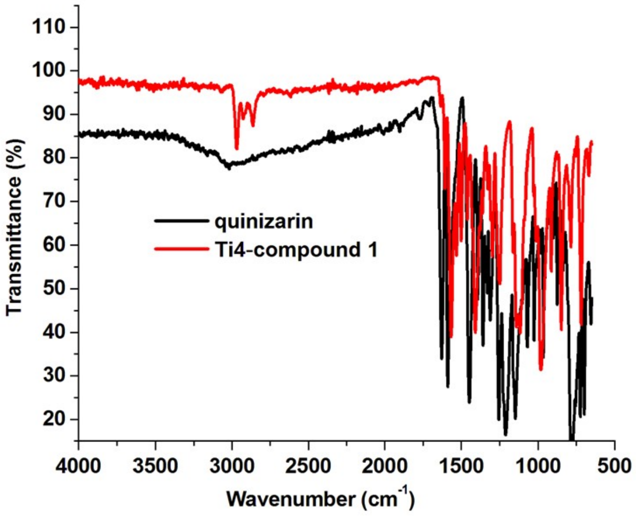

Fig. S1 The IR spectra of compound **1** and quinizarin. The presence of the quinizarin and isopropanol ligands is confirmed by the peaks in the 3100 - 3000 cm^{-1} and 3000 - 2850 cm^{-1} ranges, respectively.

The absence of the broad peak at 3250 cm^{-1} in the spectrum of compound **1** indicates the double-protonation of the dye ligand.

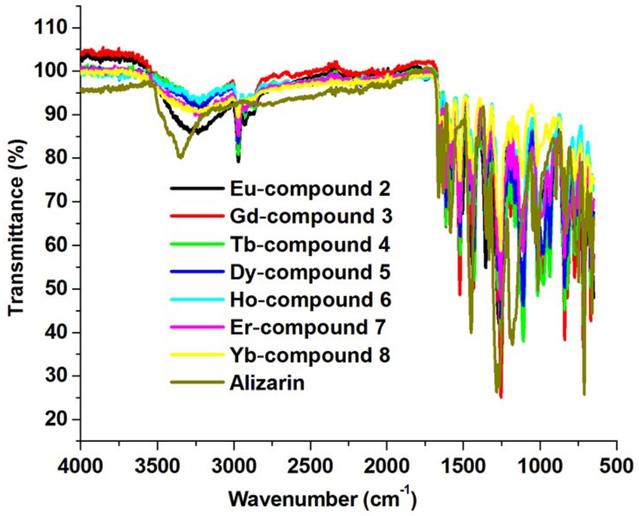

Fig. S2 IR spectra of compounds **2-8** and alizarin. The presence of the alizarin and isopropyl ligands is confirmed by the peaks in the 3100 - 3000 cm^{-1} and 3000 - 2850 cm^{-1} ranges, respectively.

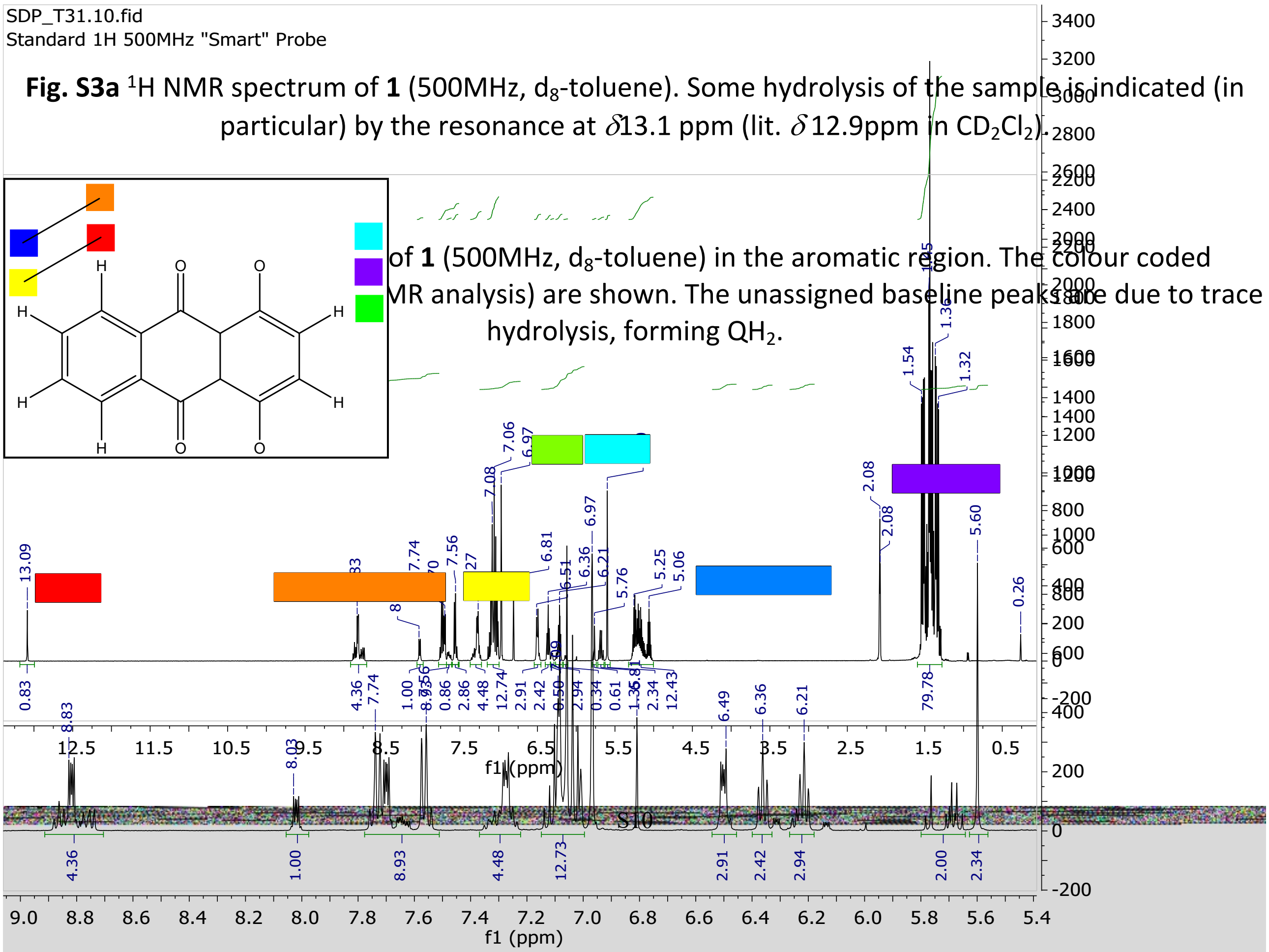

Fig. S3a ^{1}H NMR spectrum of **1** (500MHz, d_8-toluene). Some hydrolysis of the sample is indicated (in particular) by the resonance at δ13.1 ppm (lit. δ12.9ppm in CD_2Cl_2).

of **1** (500MHz, d_8-toluene) in the aromatic region. The colour coded MR analysis) are shown. The unassigned baseline peaks are due to trace hydrolysis, forming QH_2.

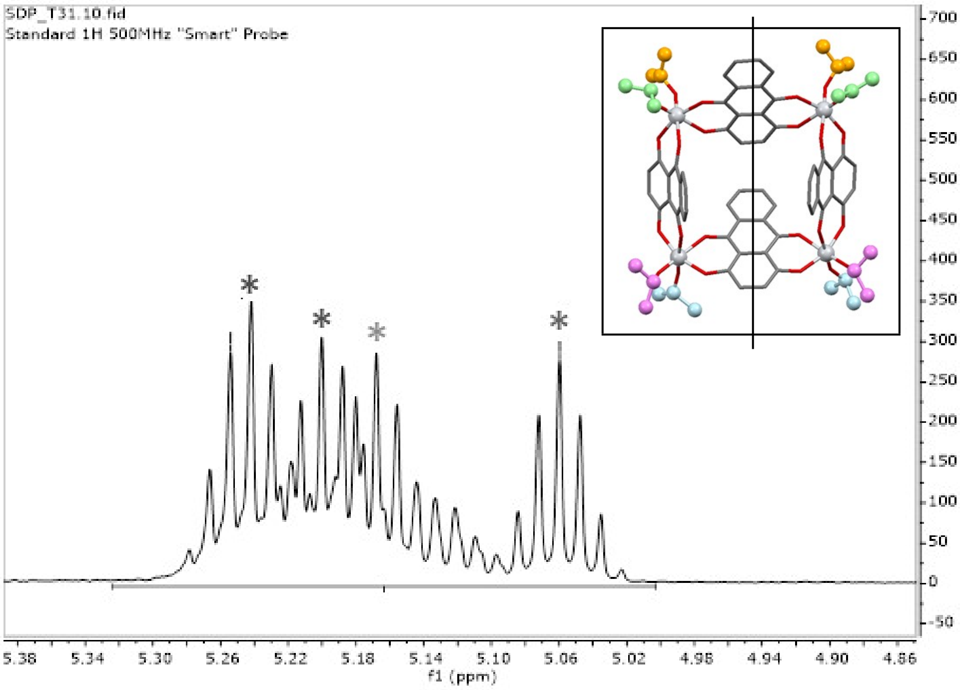

Fig. S3c ^{1}H NMR spectrum of **1** (500MHz, d_8-toluene), showing the four 1 : 1 : 1 : 1 environments. The insert shows the four ^{i}Pr environments present in the molecules (the C_s-mirror axis is also shown).

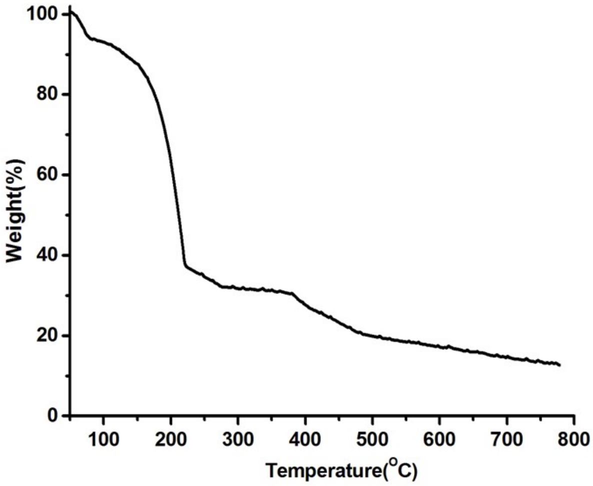

Fig. S4 The TGA curve of compound **1** (in air) TGA curves can be approximately divided into two major steps of weight loss. The first weight loss of 7.52% during the first step from 50 to 150 °C is assigned to the loss of approximately two isopropanol solvent molecules (calcd. 6.91%). After 150 °C, a gradual weight loss is attributed to the removal of eight isopropanol and quinizarin ligands (calcd. 9.96%).

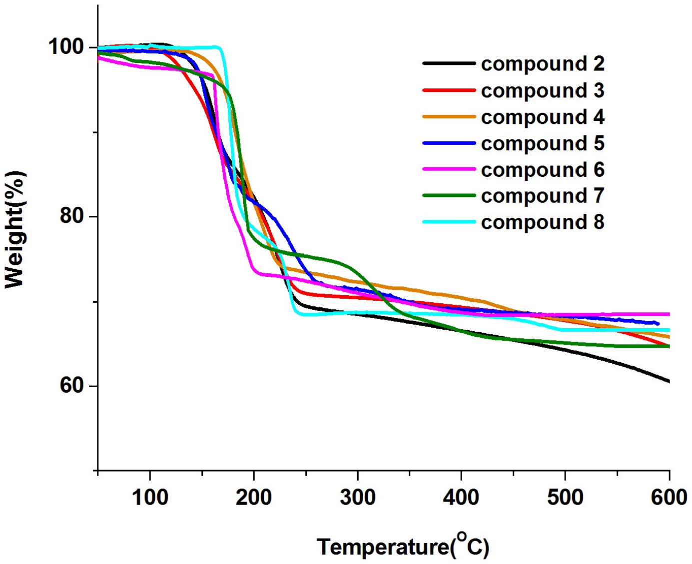

Fig. S5 The TGA curves of **2-8**. These series of compounds have similar weight loss behavior. Compounds **2-5** and **8** display one step weight loss, while compounds **6** and **7** exhibit two steps of weight loss for the presence of the isopropanol solvent.

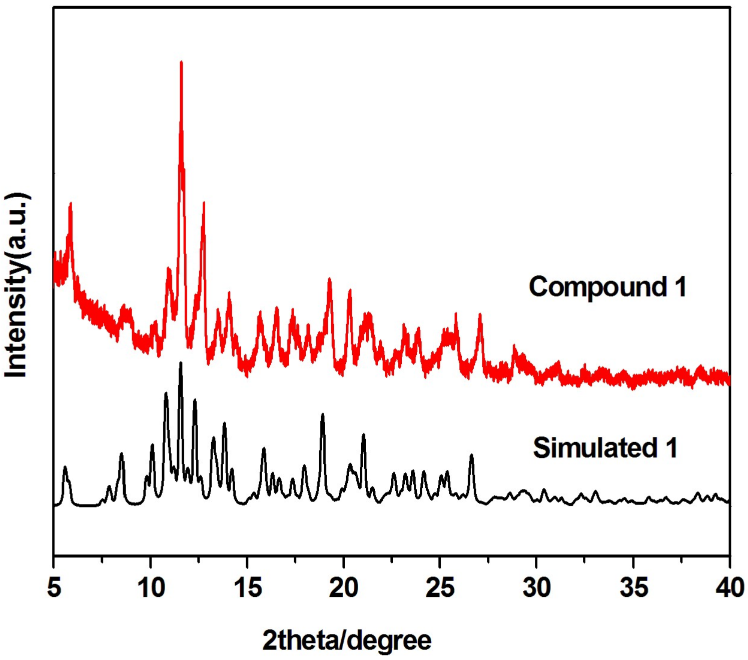

Fig. S6 Measured and simulated powder X-ray diffraction (PXRD) for compound **1**.

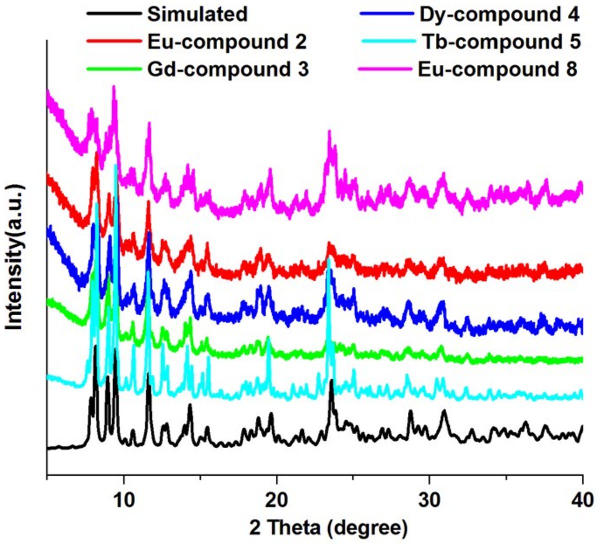

Fig. S7 The PXRD of the simulated and experimental pattern for compounds **2-5** and **8**. (Crystals containing no ^{i}PrOH lattice solvent).

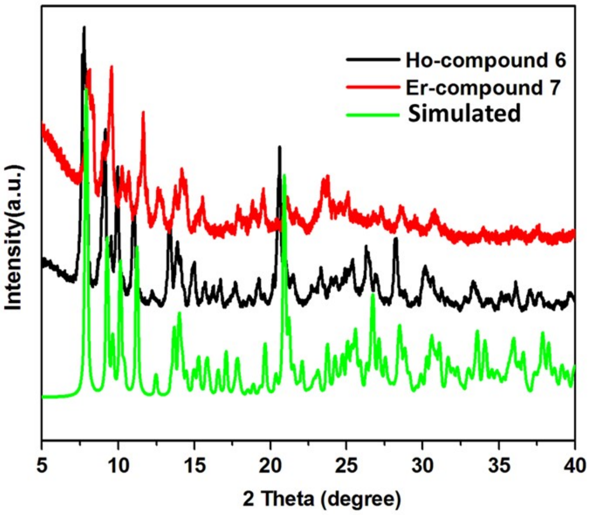

Fig. S8 The PXRD of the simulated and experimental pattern for compounds **6** and **7** (Crystals containing one ^{i}PrOH lattice solvent per formula unit).

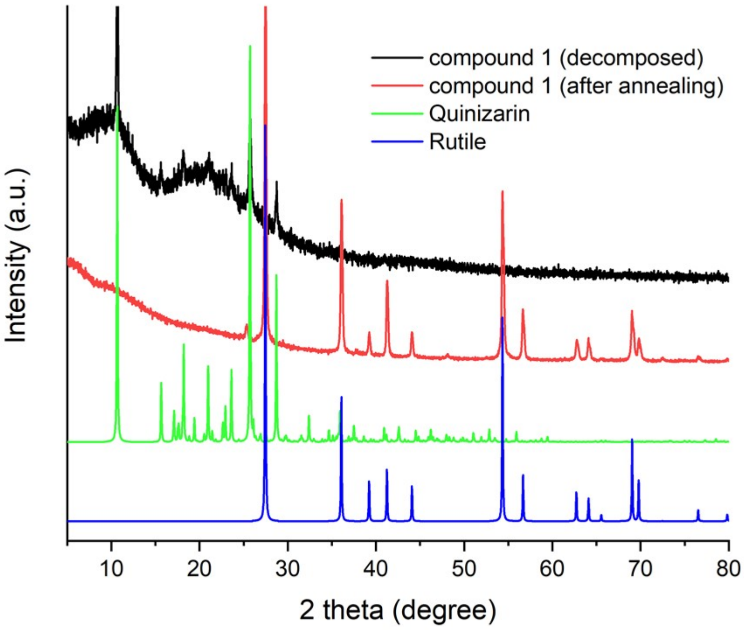
compound 1 (decomposed)
compound 1 (after annealing)
Quinizarin
Rutile
Intensity (a.u.)
10
20
30
40
50
60
70
80
2 theta (degree)

Fig. S9 The PXRD of a sample of compound **1** Initially decomposed for 16 h in a stirred CH_2Cl_2 solution in air (black line).

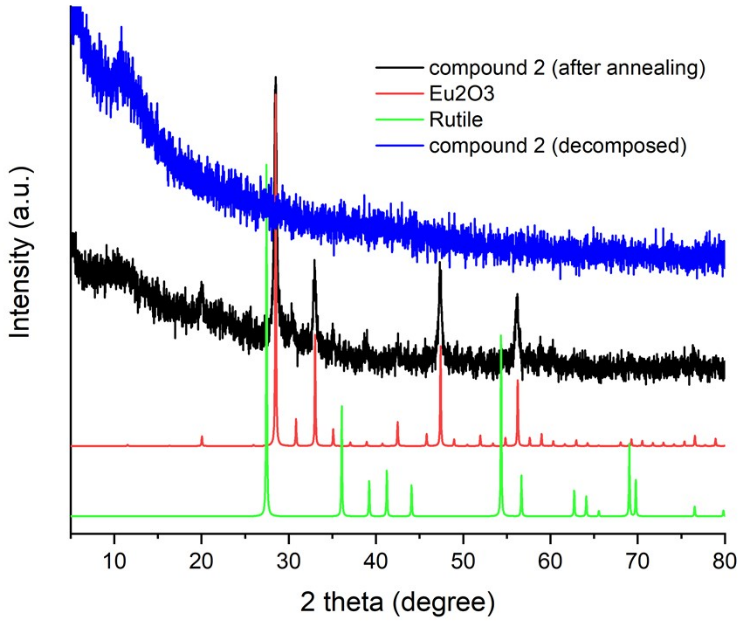

Fig. S10 The PXRD of a sample of compound **2** Initially decomposed for 16 h in a stirred CH$_2$Cl$_2$ solution in air (blue line).

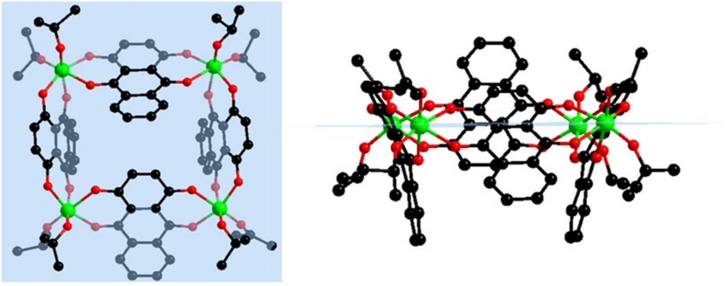

Fig. S11 The top and side view of compound **1**. Colour codes for atoms: Ti-green; O red; C-black. Selected bond lengths (Å) and angles (^{o}): [A]O-Ti range 1.925(8)-2.149(6), ^{i}PrO-Ti range 1.714(8)-1.801(6), [A]O-Ti-O[A] range 80.0(2)-82.5(2).

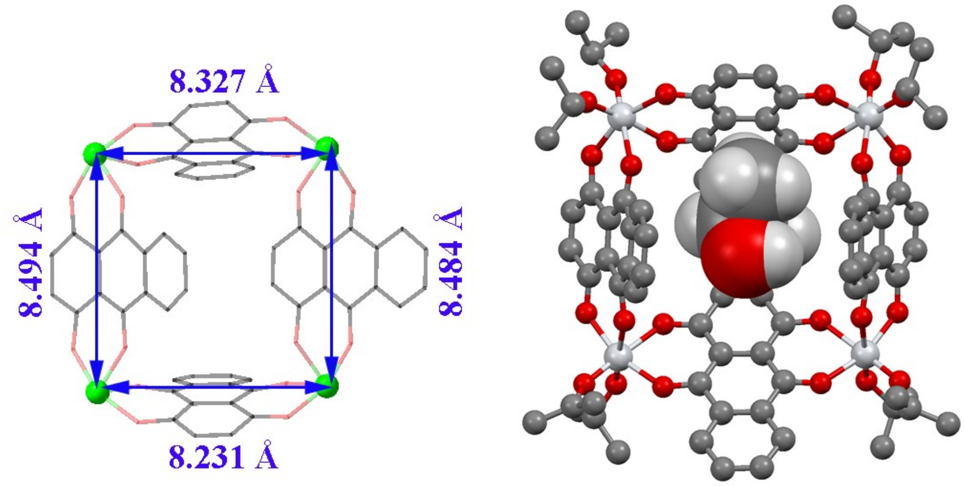

Fig. S12 (a) The dimensions of the nearly square Ti_4 cluster. (b) The trapped $^{i}PrOH$ molecule in the cavity of **1** (the trapping of the iPrOH solvent molecule is supported by C-H…arene and O-H…arene interaction).

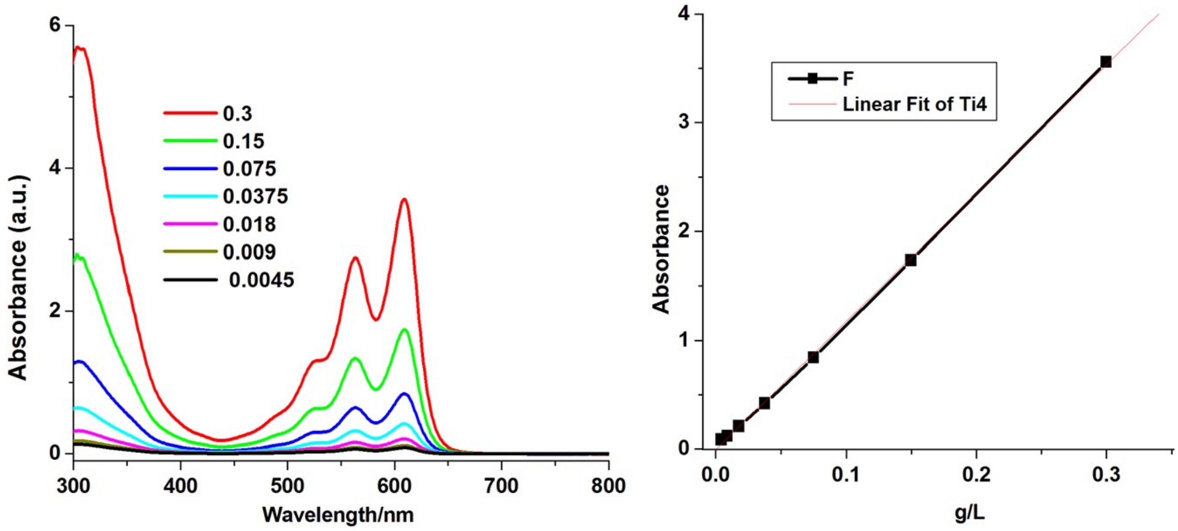

Fig. S13 (left) The UV-vis spectra of various concentrations of compound **1** in CH_2Cl_2; (right) The absorbance at 608 nm as functions of y = -0.00528 + 11.78929 x, R = 0.99974 (showing Beer-Lambert behavior).

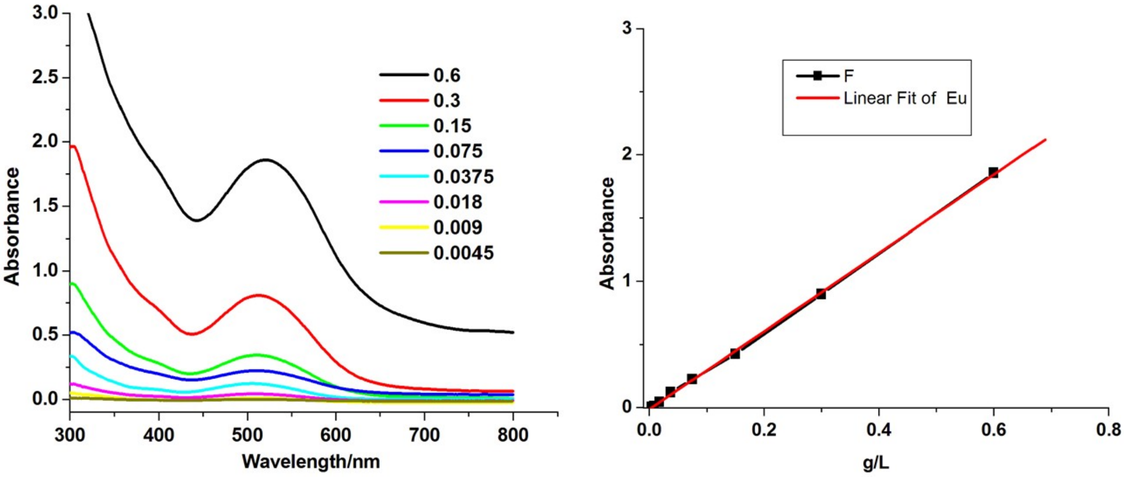

Fig. S14 (left) The UV-vis spectra of various concentrations of compound **2** in CH_2Cl_2; (right) The absorbance at 516 nm as functions of y = -0.01606 + 3.09842 x, R = 0.99973 (showing Beer-Lambert behavior).

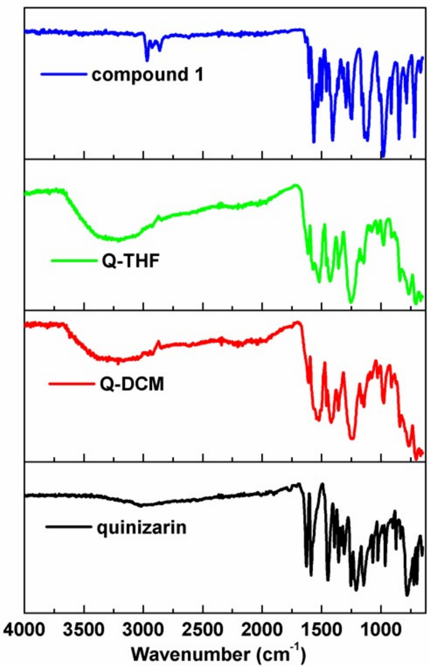

Fig. S15 The IR spectra of quinizarin (black), compound **1** in the form of solid powders (blue) and the drop-cast films from aqueous THF (green) and DCM (red).

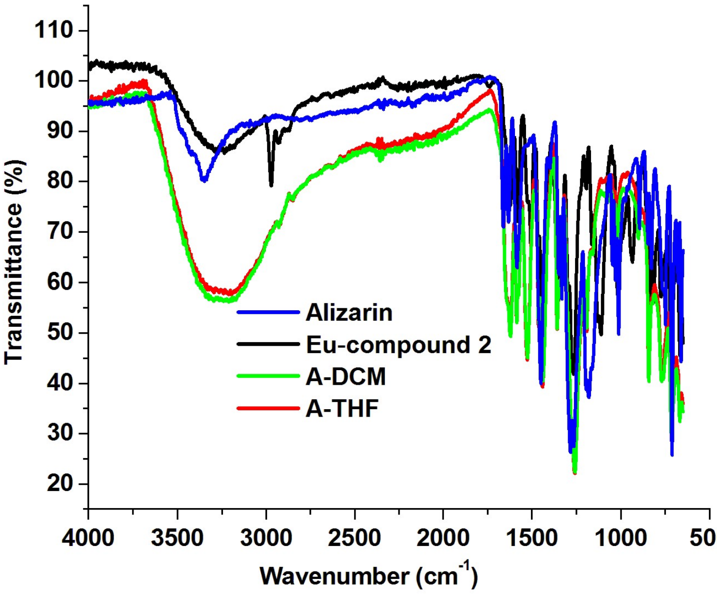
Transmittance (%)
110
100
90
80
70
60
50
40
30
20
4000
3500
3000
2500
2000
1500
1000
500
Wavenumber (cm^{-1})
Alizarin
Eu-compound 2
A-DCM
A-THF

Fig. S16 The IR spectra of alizarin, compound **2** in the form of a solid powder (black), alizarin (blue), and drop-cast films in aqueous THF (red) and DCM (green).

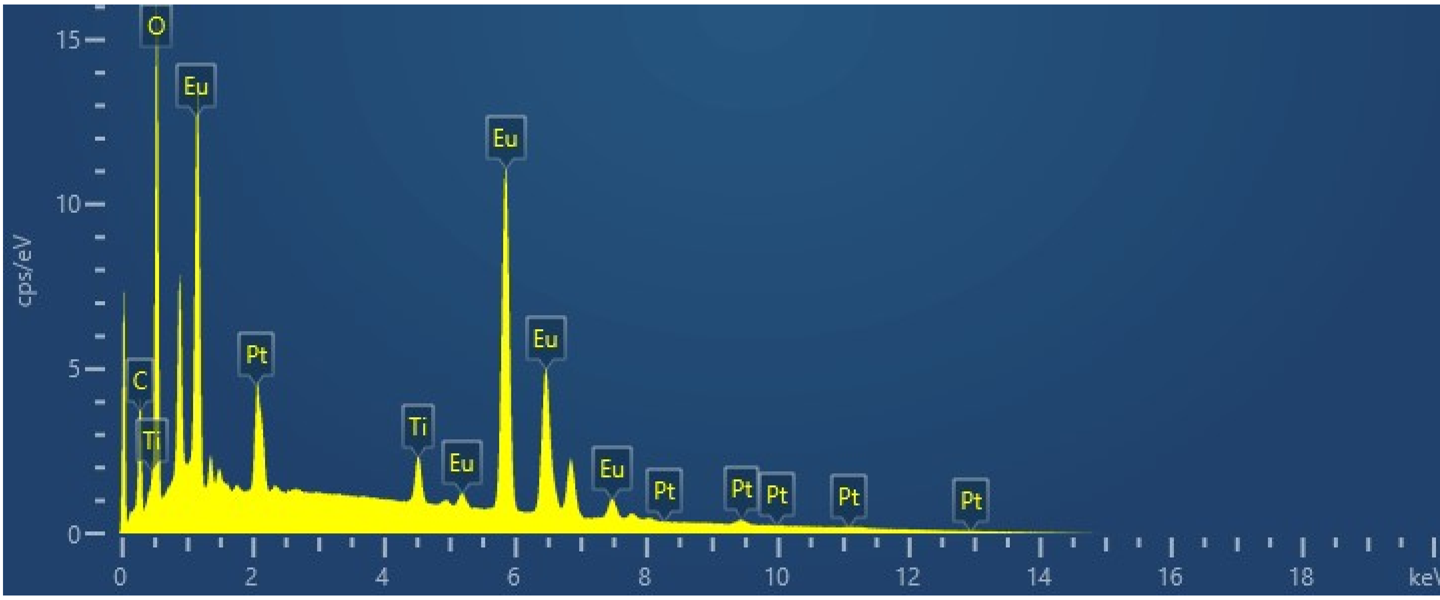

Fig. S17 Map EDX spectrum (image 1) of decomposed compound **2** after hydrolytic decomposition and annealing on carbon tape (800^{o}C), coated with 10 nm platinum. Averaged atomic percentages for relevant elements: O 41.18%, Eu 25.38% Eu, Ti 4.36%. Expected oxygen percentage for a TiO_2/Eu_2O_3 (1:1) composition: 46.79%.

Layered Imagine Side 1

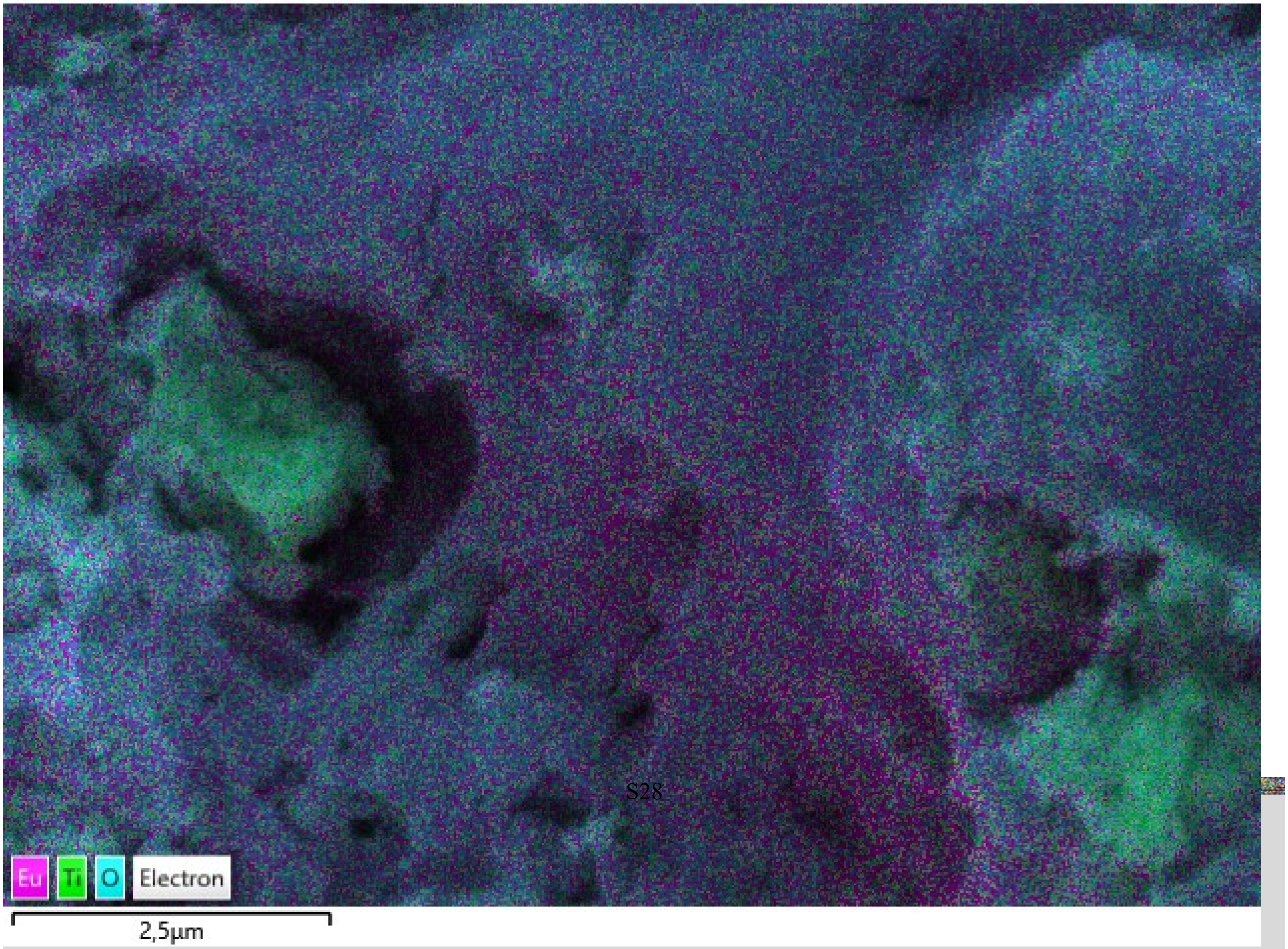

Fig.S18 Layered SEM image of image **1** including element distribution.

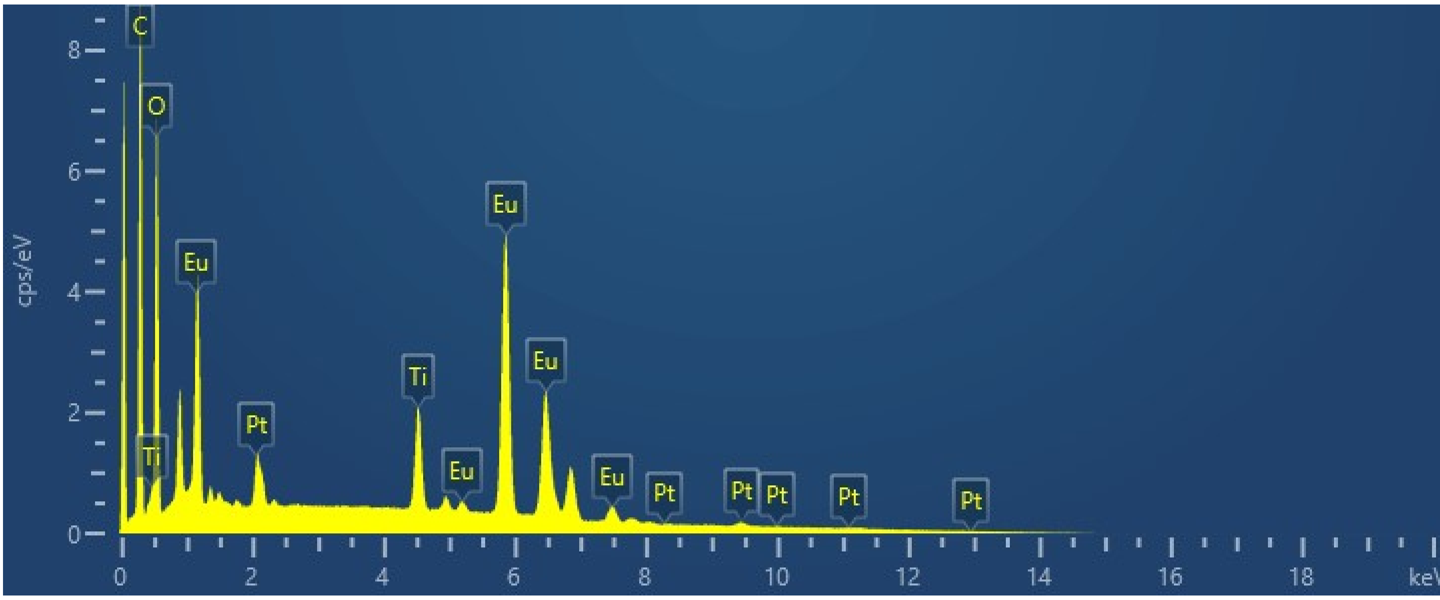

Fig. 19 Map EDX spectrum (image 2) of decomposed compound **2** after hydrolytic decomposition and

annealing on carbon tape (800^{o}C), coated with 10 nm platinum. Averaged atomic percentages for relevant elements: O 23.89%, Eu 13.82% Eu, Ti 3.15%. Expected oxygen percentage for a TiO_2/Eu_2O_3 (1:1) composition: 27.03%.

EDS Layered Image 2

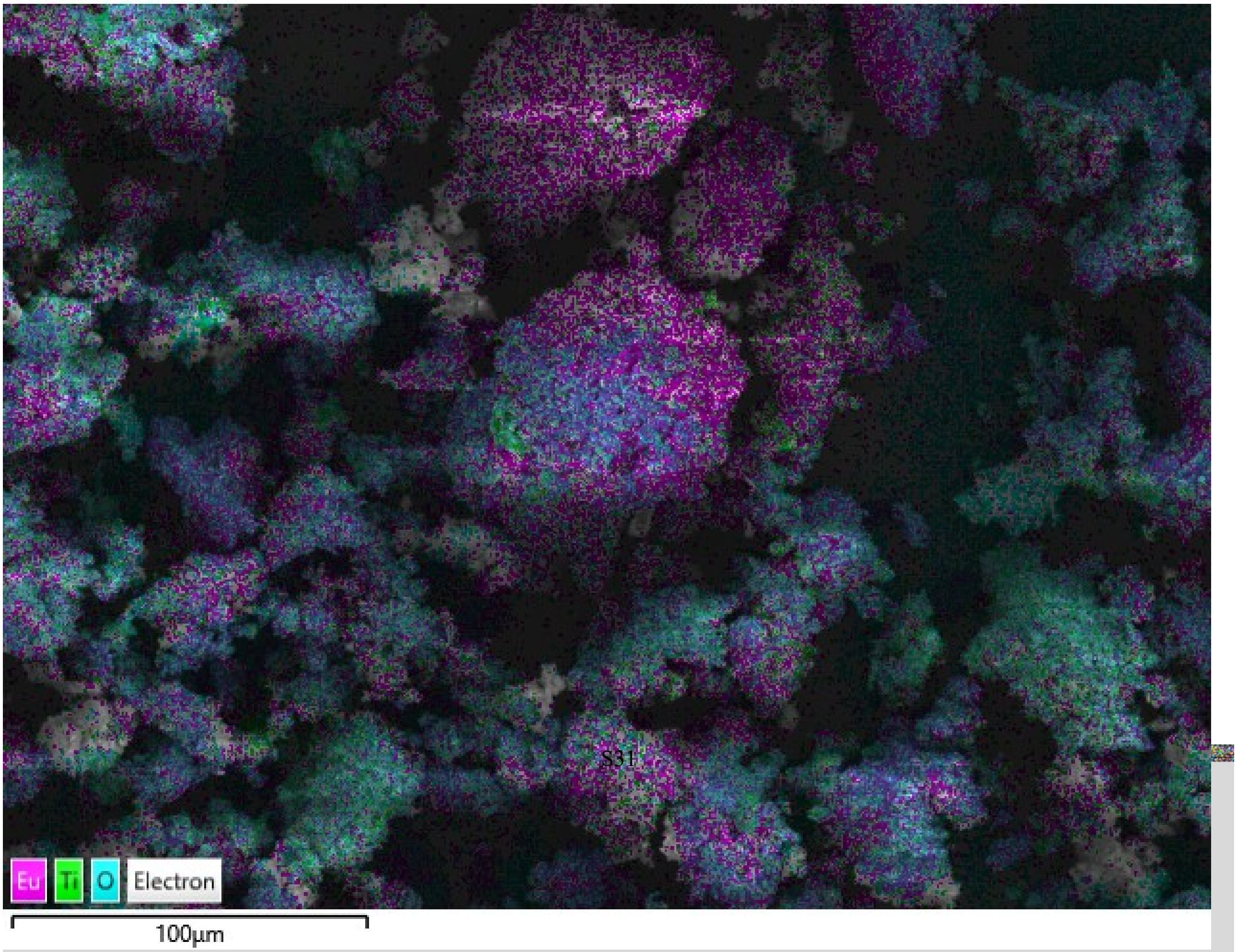

Fig. S20 Layered SEM image of image 2 including element distribution.

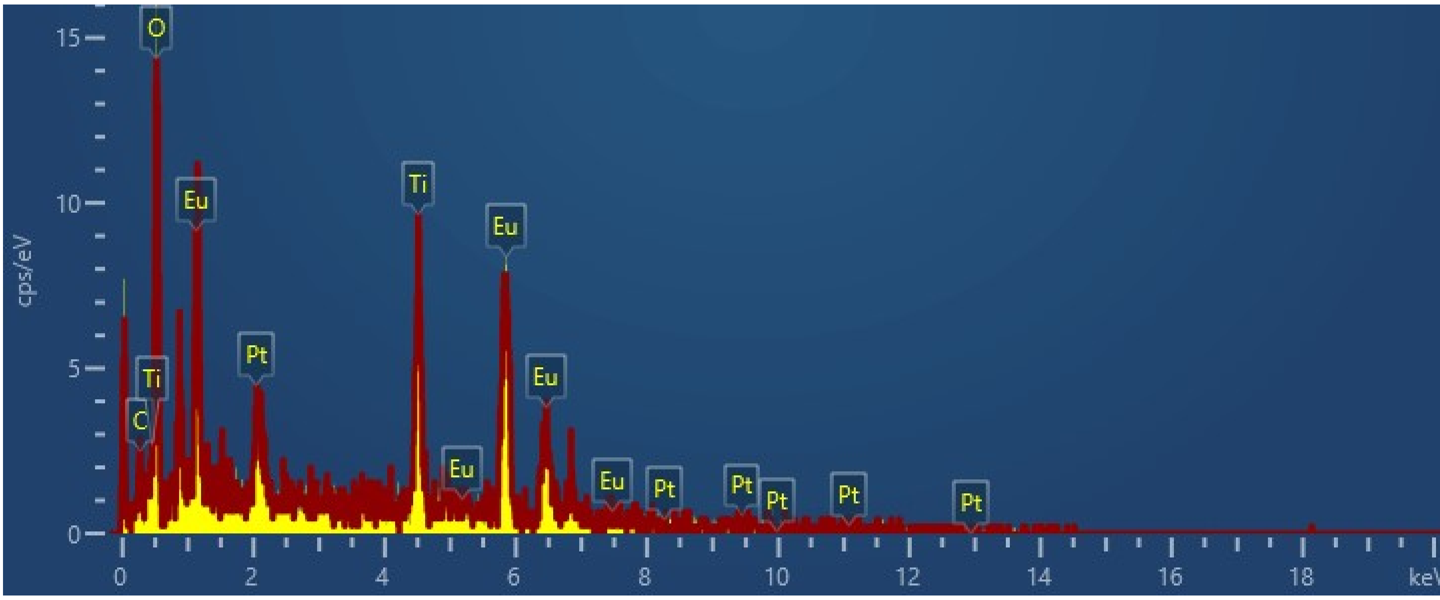

Fig. S21 Map EDX spectra of the two selected regions (images 1 and 2) of decomposed compound **2**

after annealing showing the significant variation in element distribution. Values vary as follows: O 37.21-54.17%, Eu 20.47-42.27%, Ti 4.09-13.08%, suggesting inhomogeneity of the sample.

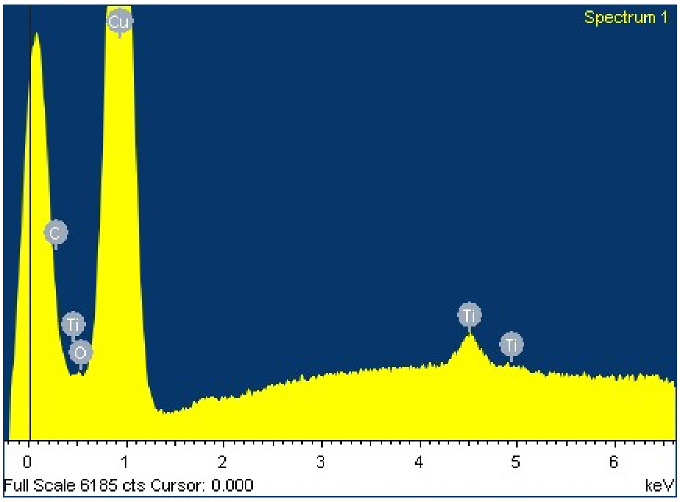

Fig. S22 The EDX spectra of brass|**1**. Compound **1** dissolved in CH_2Cl_2 (0.3 g/L) dropped onto brass.

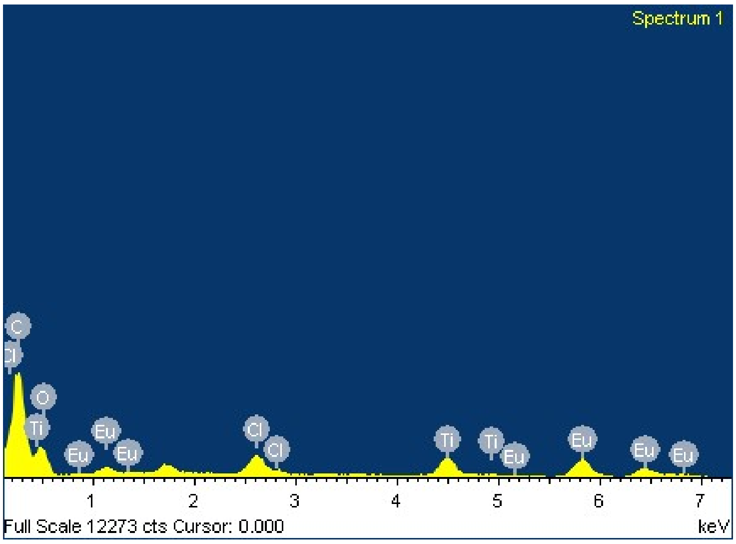

Fig. S23 The EDX spectra of FTO|**2**. Compound **2** dissolved in CH_2Cl_2 (0.3 g/L) then dropped onto brass.

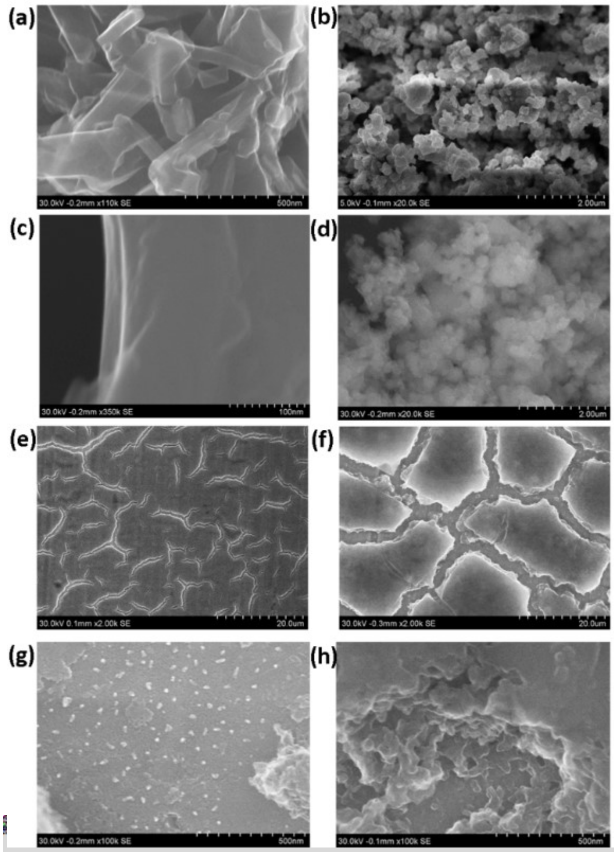
(a)
30.0kV -0.2mm x110k SE
500nm
(b)
5.0kV -0.1mm x20.0k SE
2.00um
(c)
30.0kV -0.2mm x350k SE
100nm
(d)
30.0kV -0.2mm x20.0k SE
2.00um
(e)
30.0kV 0.1mm x2.00k SE
20.0um
(f)
30.0kV -0.3mm x2.00k SE
20.0um
(g)
30.0kV -0.2mm x100k SE
500nm
(h)
30.0kV -0.1mm x100k SE
500nm

Figure S24 SEM images of the prepared materials at room temperature: (a) drop-cast FTO|**1** in THF film; (b) drop-cast FTO|**2** in THF film; (c) drop-cast FTO|**1** in DCM film; (d) drop-cast FTO|**2** in DCM film; (e) drop-cast brass|**1** in THF film; (f) drop-cast brass|**2** in THF film; (g) drop-cast brass|**1** in THF/HCl film; (h) drop-cast brass|**2** in THF/HCl.

The solubility of the compounds in common organic solvents such as toluene, dichloromethane and THF, made them amenable to drop casting. Hydrolytic deposition of the films on fluorinated tin oxide (FTO) was undertaken using **1** and the Eu compound **2** alone. In a typical procedure, dilute solutions of **1** or **2** were dropped onto the substrate and dried in air for a few hours under ambient conditions, the hydrolytic decomposition of the complexes resulting from atmospheric moisture. A selection of solvents was tested in order to investigate the morphologies of the resulting films. As observed by SEM, drop-cast samples on FTO at room temperature exhibit a nearly uniform distribution (Figure S24). However, **1** and **2** display different film morphologies when drop-cast from THF solution. The magnified images show that **1** exhibits a plate-like morphology (Figure S24a) while compound **2** generates a porous micro-particle morphology (Figure S24b), both morphologies being similar to the initial shapes of the crystalline precursors prior to hydrolysis, as observed by SEM. When drop-cast from dichloromethane, the morphology of **1** changes to a smooth layer morphology, with layer thickness about 10 nm (Figure S24c), while for compound **2**, a porous nano-particulate morphology is retained (Figure S24d).

In addition to the solvent, the substrate and the pH at which hydrolysis occurs both influence the morphology of deposited films. For example, deposition from THF solutions onto a brass substrate produced thick (cracked) layers for both **1** and **2** (Figures S24e and S24f).

Adding a few drops of aqueous HCl (pH 2) to the THF solutions of **1** and **2**, in order to accelerate decomposition, p24oduced uniform nanoparticles on brass in the case of **1** (ca. 10-20 nm in diameter) (Figure S24g), with compound **2** giving a porous morphology (Figure S24h).

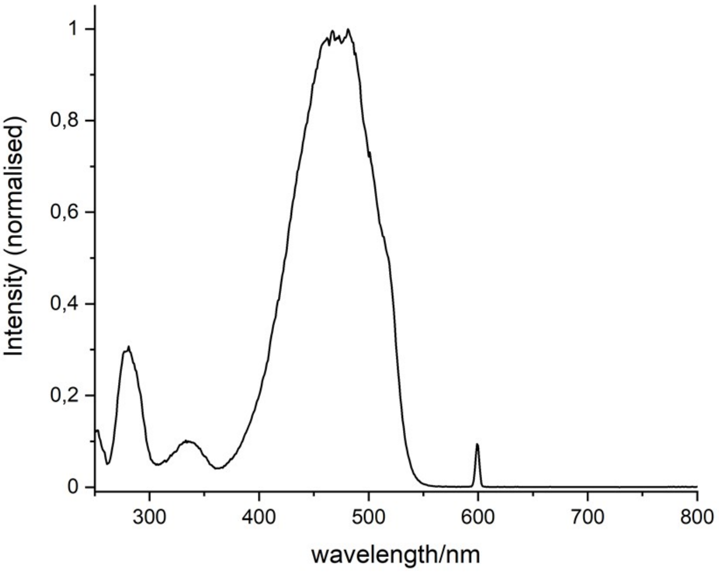

Fig. S25 Excitation spectrum of compound **1** in dry CH_2Cl_2. The detected emission was set to 530 nm.

The maximum at 480 nm was used as excitation wavelength for further emission measurements.

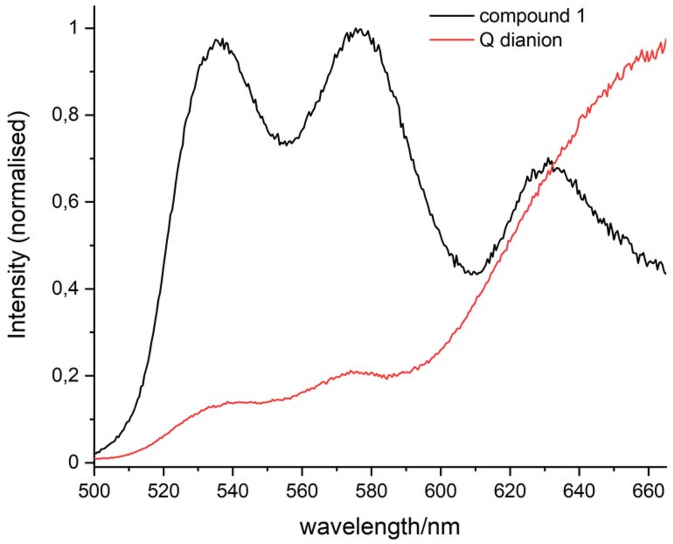

Fig. S26 Emission spectrum of compound **1** (dry CH_2Cl_2) and the dianion of quinizarin (water) at 480 nm excitation.

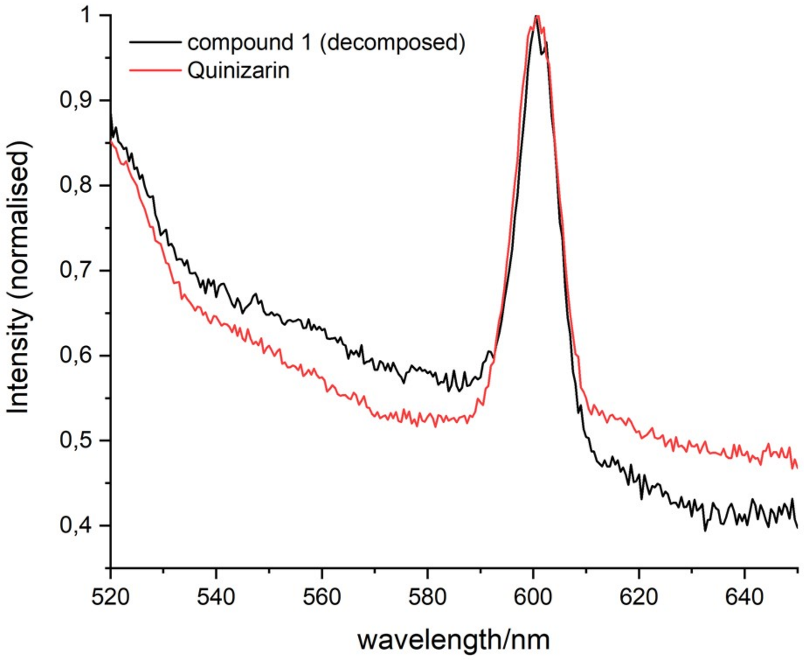
compound 1 (decomposed)
Quinizarin
Intensity (normalised)
1
0,9
0,8
0,7
0,6
0,5
0,4
520
540
560
580
600
620
640
wavelength/nm

Fig. S27 Solid state emission spectra of decomposed compound **1** (before annealing) and quinizarin. Overlapping of the peaks proves the liberation of quinizarin molecules upon decomposition

4. Cyclic Voltammetry on 1

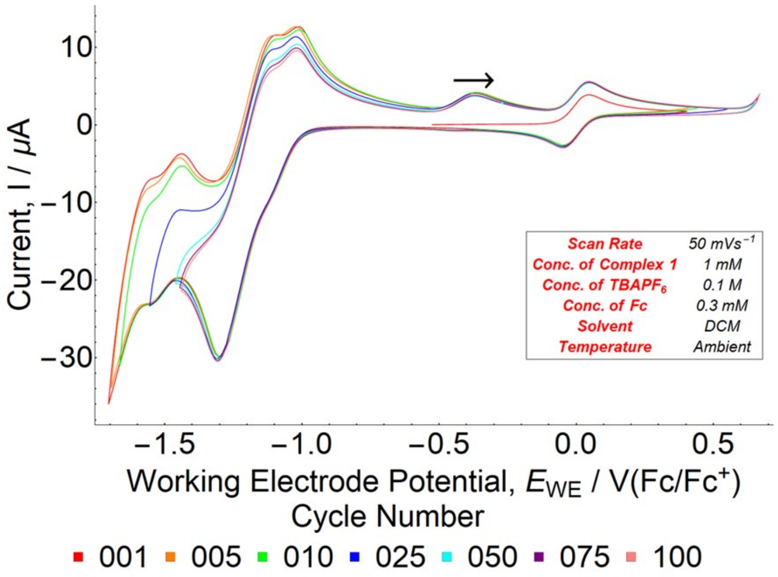
Current, I / μA
10
0
−10
−20
−30
−1.5
−1.0
−0.5
0.0
0.5
Working Electrode Potential, E_{WE} / V(Fc/Fc$^+$)
⟶
Scan Rate 50 mVs^{-1}
Conc. of Complex 1 1 mM
Conc. of TBAPF$_6$ 0.1 M
Conc. of Fc 0.3 mM
Solvent DCM
Temperature Ambient
Cycle Number
001 005 010 025 050 075 100

Fig. S28 *(Above)* CV of Species **1** in dry dichloromethane with 0.1 M $TBAPF_6$ and 0.3 mM Ferrocene. *(Below)* Images of the deposit in the electrochemical cell and on the surface of the working electrode

As can be seen from the cyclic voltammetry, for compound **1** there appears to be an irreversible oxidation at -0.37 V (Fc/Fc^+) that persists over the course of 100 cycles. Since it is not present at the beginning of the first cycle, it is likely to be related to a reductive process at a lower potential. It must be noted that this oxidation is also observed when quinizarin is tested (Figure S30).At lower potentials, there is a more complex shape comprising of an asymmetric set of reductive and oxidative waves. Regarding reduction, there is one clear reductive peak at -1.30 V (Fc/Fc$^+$) and two weaker ones at -1.10 V (Fc/Fc$^+$) and -1.55 V (Fc/Fc$^+$); the oxidative peaks can be found at -1.44 V (Fc/Fc$^+$), -1.10 V (Fc/Fc$^+$) and -1.01 V (Fc/Fc$^+$). Assuming the closest sequential, by potential, oxidative and reductive waves are redox couples then the relative peak separations from high to low potential are 83 mV, 187 mV and 95 mV respectively as you move to lower potential. A reversible single-electron process is expected to have a peak width of 57 mV [N. Elgrishi, K. J. Rountree, B. D. McCarthy, E. S. Rountree, T. T. Eisenhart, J. L. Dempsey, *J. Chem. Educ.* **2018**, *95*, 197-206] but may be higher if solution resistance effects are involved [C. Amatore, A. Oleinick, I. Svir, *Anal. Chem.* **2008**, *80*, 7957-7963]. However, while the first couple may appear reversible from the width alone, the asymmetry of the peak currents in the CV would suggest otherwise. It could be suggested that the reduction at -1.30 V pairs with the oxidative couples at -1.1 and -1.0 V. This would give a peak width of ~200 mV and suggest a large degree of polarisation in the electrochemical process. Deposition on the working electrode and cell-walls was observed after the termination of the experiment suggesting degradation of the compound or lack of solubility of the reduced product in the supporting electrolyte solution. The loss of the low potential processes over the course of the cycling is a result of the drift in the electrochemical window due to the pseudo-reference used. Although, the oxidative peaks do appear to diminish in current intensity over the course of the 100 cycles while the reductive peaks largely remain intact.

For cycle 25 (blue), we see the loss of the low potential reduction and oxidation processes. This is likely to be due to the drift of the electrochemical window cutting off the low potential reduction and so the related oxidation is therefore not observed subsequently.

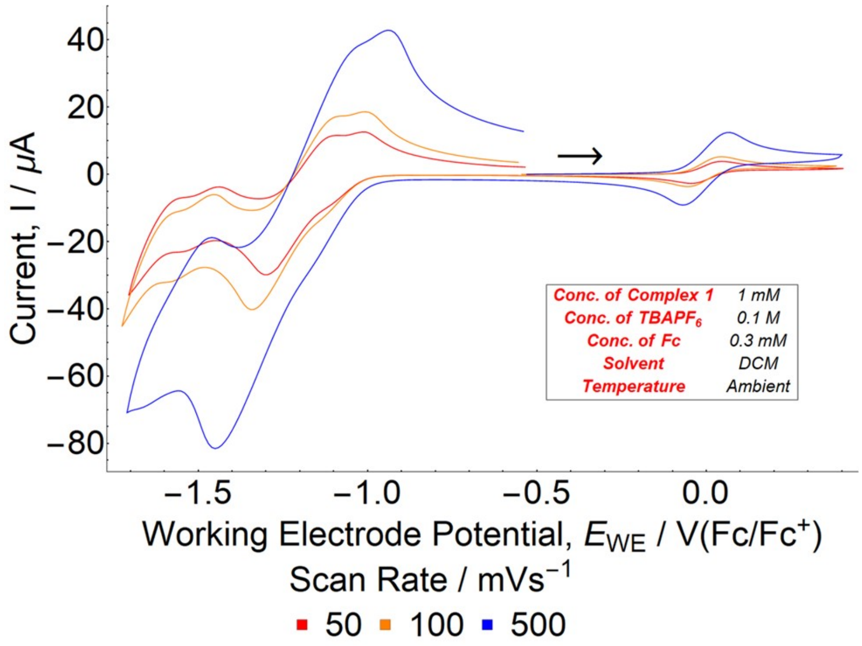
Current, I / μA
40
20
0
−20
−40
−60
−80
−1.5
−1.0
−0.5
0.0
Working Electrode Potential, E_WE / V(Fc/Fc⁺)
⟶
Conc. of Complex 1 1 mM
Conc. of TBAPF₆ 0.1 M
Conc. of Fc 0.3 mM
Solvent DCM
Temperature Ambient
Scan Rate / mVs⁻¹
■ 50 ■ 100 ■ 500

Figure S29 CV of Species **1** in dry dichloromethane with 0.1 M TBAPF$_6$ and 0.3 mM Ferrocene at varied scan rates.

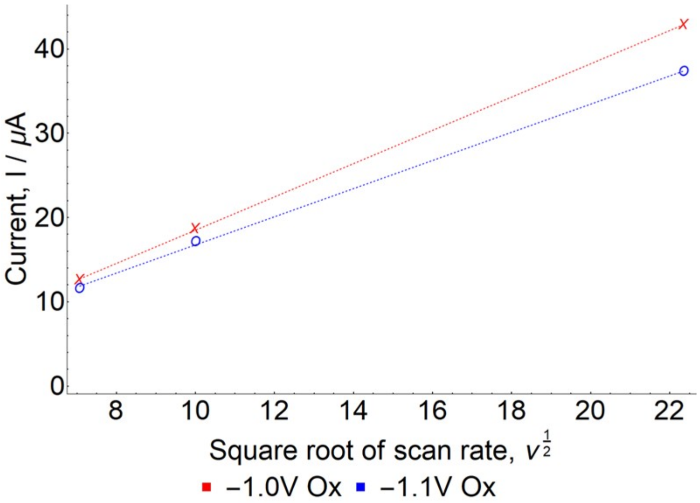

Red line = -1.23367 + 1.97349X, R^2 = 0.99994
Blue line = 0.0532401 + 1.66983X, R^2 = 0.999441

While **1** contains four quinizarin molecules within its structure, the electrochemical behaviour is different when compared to the lone anthraquinone ligand. This may be due to some degree of charge delocalisation occurring during the electrochemical process so that the cyclic voltammogram produced is a result of that more complex interaction.

Quinizarin in DCM appears to demonstrate two, 1-electron processes (-1.17 and -1.61 V (Fc/Fc$^+$)) as can be seen in the diagram below. Over the course of 100 cycles, the first couple (-1.17 V (Fc/Fc$^+$)) shows signs of degradation over the course of 100 cycles with the growth of a peak at -0.345 V and the decrease in the currents produced in the peak at -1.13 V (Fc/Fc$^+$). The peak widths, referring to the higher potential peak first, at 50 mVs^{-1} found are ~85 mV and ~80 mV for the two peaks.

In complex **1**, however, quinizarin is not fully protonated but has deprotonated hydroxy groups. To investigate the behaviour of the deprotonated anthraquinone, CV was also carried in 1M KOH in aqueous solution. Here the behaviour was different from in DCM whereby a single two-electron redox couple (-0.66 V (Hg/HgO)) could be observed in place of two single-electron processes. The peak width at 50 mVs^{-1} was 65 mV.

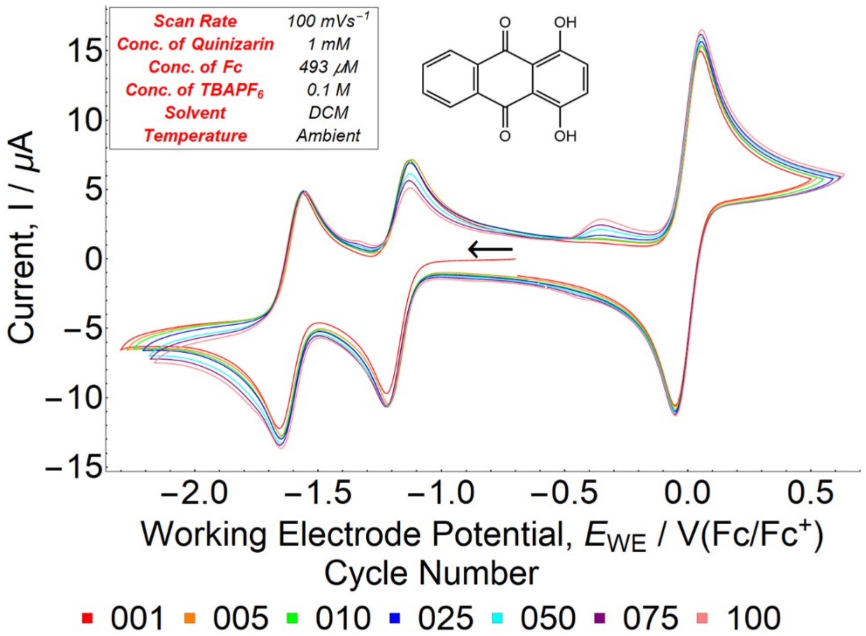

Figure S30 Cyclic voltammograms of quinizarin in DCM spanning cycles 1-100.

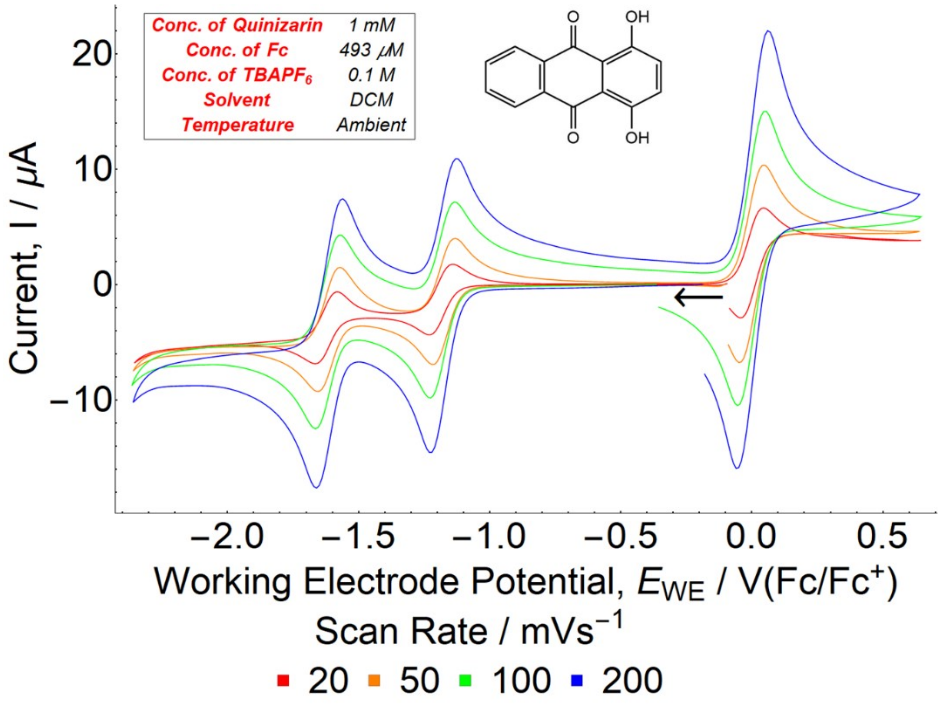
Conc. of Quinizarin 1 mM
Conc. of Fc 493 μM
Conc. of TBAPF6 0.1 M
Solvent DCM
Temperature Ambient
O
OH
O
OH
Current, I / μA
20
10
0
−10
−2.0
−1.5
−1.0
−0.5
0.0
0.5
Working Electrode Potential, EWE / V(Fc/Fc+)
Scan Rate / mVs−1
20
50
100
200

Figure S31 Cyclic voltammograms of quinizarin in DCM showing the first cycle at different scan rates ranging from 20-200 mVs^{-1}.

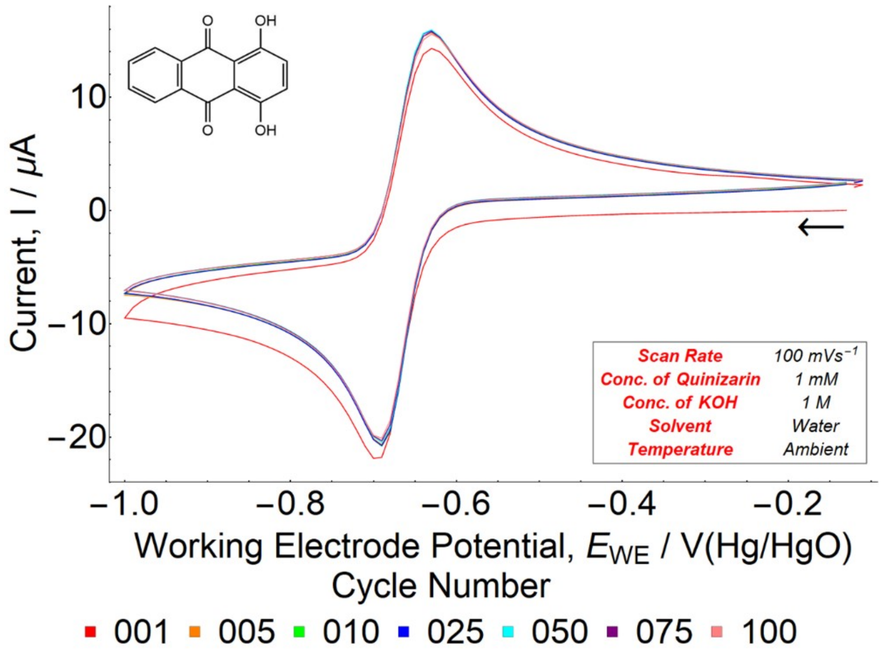

Figure S32 Cyclic voltammograms of quinizarin in 1M KOH aqueous solution spanning cycles 1-100.

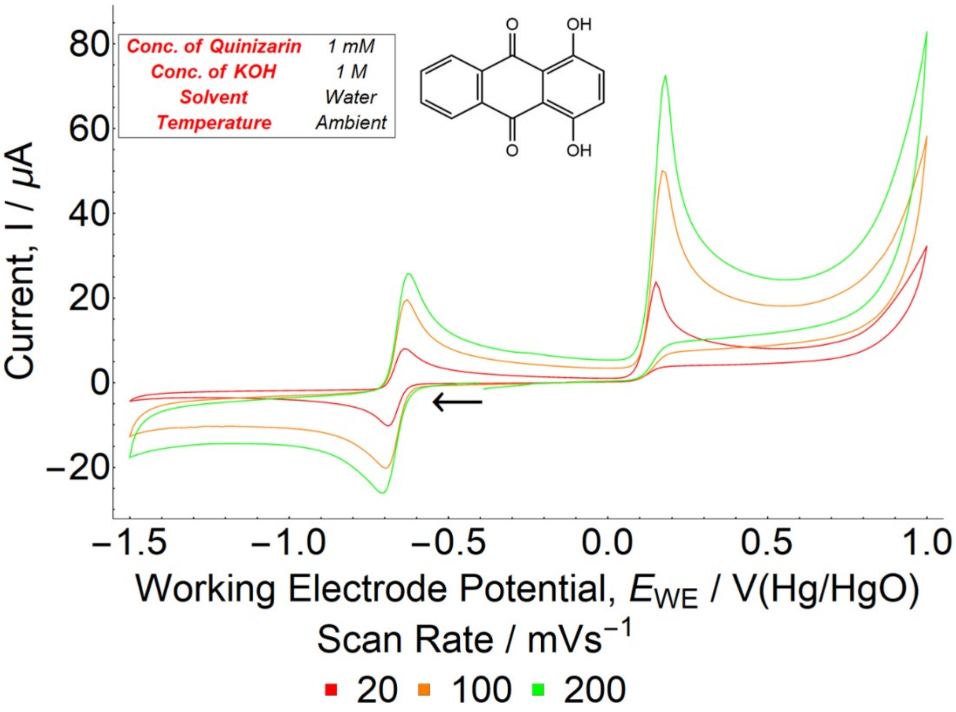
Conc. of Quinizarin 1 mM
Conc. of KOH 1 M
Solvent Water
Temperature Ambient
O
OH
O
OH
80
60
40
20
0
−20
Current, I / μA
−1.5
−1.0
−0.5
0.0
0.5
1.0
Working Electrode Potential, E_WE / V(Hg/HgO)
Scan Rate / mVs⁻¹
20
100
200

Figure S33 Cyclic voltammograms of quinizarin in 1M KOH aqueous solution showing the first cycle at different scan rates ranging from 20-200mVs^{-1}.

X-Ray Crystallography

Compound 1: The X-ray data show a rapid drop off in intensity, falling below $3\sigma(I)$ around 1.0 Å. For refinement, the data are truncated to 0.95 Å, with ca 62% observed at the $2\sigma(I)$ level to that resolution. The structure of the primary Ti_4 complex is clear. All atoms are refined with anisotropic ADPs, but with ISOR restraints applied to the C atoms. It may be possible to model some of the coordinated isopropyl molecules with split-atom sites, but this adds little to the model, so was not implemented. The ^{i}PrOH molecule trapped within the Ti_4 complex is relatively clear. It is refined with a restrained geometry and a single common isotropic ADP (which is large). The electron density indicates further solvent molecules around 0.525,-0.139,0.598 and 0.248,0.282,0.979, but these could not easily be defined as isopropyl molecules, so they were omitted and SQUEEZE has been applied. SQUEEZE corrects for a total of 244 electrons per unit cell, which approximates 8 ^{i}PrOH molecules (= 272 electrons), in addition to the 8 ^{i}PrOH molecules that are included in the model. This is in good agreement with thermogravimetic analysis and elemental analysis, which indicate two ^{i}PrOH molecules per $Ti_4(L_1)_4(O^iPr)_8$ unit.

Compounds 2, 3, 4, 5, 8: These five crystal structures are isomorphous. Refinement was largely straightforward. All atoms are refined with anisotropic ADPs, but with ISOR restraints applied to all O and C atoms. Geometrical restraints were applied to all of the coordinated isopropyl molecules. It may be possible to model some of these with split-atom sites, but it was considered that this would add little to the model, so was not implemented. The H atoms on O for the coordinated ^{i}PrOH molecules (clearly evident from the Ti—O distances) were added along the O···Cl vector to make reasonable H-bonds and allowed to ride on their parent atoms. For **5**, the X-ray data show a rapid drop off in intensity, falling below $3\sigma(I)$ around 1.05 Å. For refinement, the data are truncated to 0.95 Å, with ca 60% observed at the $2\sigma(I)$ level to that resolution.

Compounds 6, 7: These crystal structures are isomorphous. In both structures, two isopropyl ligands are modelled as disordered with two components. The C atoms of these disorder components are refined with isotropic ADPs. For **6**, the H atoms on O for the coordinated ^{i}PrOH molecules were visible in the different Fourier map. They were included in their as-found positions and allowed to ride on their parent atoms. For **7**, the H atoms were added along the O···Cl vector to make reasonable H-bonds.

Table S1. Crystallographic details for compounds 1-8

	1_squeeze	**2**	**3**	**4**
CCDC number	1547945	1547946	1547947	1547948
Cambridge data number	SP_B1_0081	DW_B2_0246	DW_B2_0234	DW_B2_0236
Chemical formula	$C_{83}H_{88}O_{25}Ti_4$	$C_{49}H_{63}Cl_2EuO_{15}Ti_2$	$C_{49}H_{63}Cl_2GdO_{15}Ti_2$	$C_{49}H_{63}Cl_2O_{15}TbTi_2$
Formula weight	1677.13	1210.65	1215.94	1217.61
Temperature / K	180(2)	180(2)	180(2)	180(2)
Crystal system	monoclinic	triclinic	triclinic	triclinic
Space group	*I* 2/*a*	*P*–1	*P*–1	*P*–1
a / Å	30.907(3)	15.5101(3)	15.5072(3)	15.4971(4)
b / Å	17.5383(9)	15.5865(3)	15.5889(3)	15.5805(4)
c / Å	31.7979(17)	22.8777(5)	22.8805(5)	22.8741(6)
α / °	90	85.4138(12)	85.180(2)	85.1389(13)
β / °	97.233(2)	79.8656(12)	79.737(2)	79.6785(13)
γ / °	90	86.3382(11)	86.402(2)	86.4276(14)

Unit-cell volume / Å^3	17099(2)	5419.93(19)	5416.95(19)	5407.8(2)
Z	8	4	4	4
Calc. density / g cm^{-3}	1.303	1.484	1.491	1.496
F(000)	6992	2472	2476	2480
Radiation type	CuKα	CuKα	CuKα	CuKα
Absorption coeff. / mm^{-1}	3.683	12.051	11.688	10.206
Crystal size / mm^3	0.20 x 0.10 x 0.08	0.22 x 0.20 x 0.16	0.27 x 0.18 x 0.17	0.30 x 0.27 x 0.23
2θ range / °	5.60-108.48	5.70-133.66	5.70-133.73	5.70-133.59
Completeness to max 2θ	0.996	0.982	0.984	0.990
No. of refl. measured	82552	43697	41743	62819
No. of independent refl.	10429	18923	18961	19033
R_{int}	0.0780	0.0634	0.1003	0.0688
Parameters / restraints	986 / 534	1271 / 824	1271 / 824	1271 / 824
Final $R1$ values ($I > 2\sigma(I)$)	0.0999	0.0597	0.0710	0.0603
Final $wR(F^2)$ values (all data)	0.1406	0.0995	0.1333	0.0842
Goodness-of-fit on F^2	1.040	1.038	1.039	1.065

Largest difference peak & hole / e Å^{-3}	1.250, -0.546	0.921, -0.686	0.984, -0.642	1.726, -1.491

Table S1 (cont.). Crystallographic details for compounds 2-8

	5	**6**	**7**	**8**
CCDC number	1547949	1547950	1547951	1547952
Cambridge data number	DW_B2_0247	DW_B2_0233	DW_B2_0248	DW_B2_0231
Chemical formula	$C_{49}H_{63}Cl_2DyO_{15}Ti_2$	$C_{52}H_{71}Cl_2HoO_{16}Ti_2$	$C_{52}H_{71}Cl_2ErO_{16}Ti_2$	$C_{49}H_{63}Cl_2O_{15}Ti_2Yb$
Formula weight	1221.19	1283.71	1286.04	1231.73
Temperature / K	180(2)	180(2)	180(2)	180(2)
Crystal system	triclinic	monoclinic	monoclinic	triclinic
Space group	P–1	$P\,2_1/n$	$P\,2_1/n$	P–1
a / Å	15.4836(6)	21.4543(5)	21.4699(5)	15.4492(4)
b / Å	15.5960(6)	13.9595(3)	13.9439(3)	15.5949(4)
c / Å	22.9117(9)	21.5029(5)	21.5190(5)	22.9087(5)
α / °	84.978(3)	90	90	84.7357(14)
β / °	79.409(3)	117.2507(10)	117.3726(12)	79.4089(14)

γ / °	86.553(3)	90	90	86.5626(14)
Unit-cell volume / Å^3	5412.2(4)	5725.2(2)	5720.9(2)	5397.2(2)
Z	4	4	4	4
Calc. density / g cm^{-3}	1.499	1.489	1.493	1.516
F(000)	2484	2624	2628	2500
Radiation type	CuKα	CuKα	CuKα	CuKα
Absorption coeff. / mm^{-1}	11.159	6.188	6.332	6.988
Crystal size / mm^3	0.15 x 0.10 x 0.09	0.16 x 0.15 x 0.10	0.16 x 0.15 x 0.10	0.15 x 0.12 x 0.12
2θ range / °	5.69-108.48	4.82-133.59	4.81-133.27	5.70-140.72
Completeness to max 2θ	0.994	0.978	0.998	0.987
No. of refl. measured	33793	35329	41664	57159
No. of independent refl.	13164	9949	10110	20343
R_{int}	0.1184	0.0342	0.0653	0.0543
Parameters / restraints	1271 / 824	674 / 24	682 / 24	1271 / 824
Final $R1$ values ($I > 2\sigma(I)$)	0.0765	0.0376	0.0463	0.0407
Final $wR(F^2)$ values (all data)	0.1391	0.0503	0.0705	0.0626

Goodness-of-fit on F^2	1.004	1.040	1.047	1.036
Largest difference peak & hole / e Å^{-3}	1.120, -0.838	0.724, -0.526	0.726, -0.630	1.056, -0.722

Table S2. Bond lengths [Å] for compounds 2-8

Compound 2		Compound 3		Compound 4		Compound 5	
Eu1—O6	2.337(4)	Gd1—O12	2.330(5)	Tb1—O6	2.314(4)	Dy1—O6	2.284(8)
Eu1—O12	2.346(4)	Gd1—O6	2.330(5)	Tb1—O12	2.317(4)	Dy1—O12	2.311(7)
Eu1—O2	2.359(4)	Gd1—O7	2.350(5)	Tb1—O7	2.319(4)	Dy1—O2	2.318(7)
Eu1—O7	2.359(4)	Gd1—O2	2.351(5)	Tb1—O2	2.338(4)	Dy1—O7	2.328(8)
Eu1—O1	2.400(4)	Gd1—O1	2.387(5)	Tb1—O1	2.384(4)	Dy1—O1	2.394(7)
Eu1—Cl1	2.6802(18)	Gd1—Cl1	2.667(2)	Tb1—Cl1	2.6537(17)	Dy1—Cl1	2.641(3)
Eu1—Cl2	2.6978(17)	Gd1—Cl2	2.681(2)	Tb1—Cl2	2.6652(16)	Dy1—Cl2	2.661(3)
Eu2—O21	2.349(5)	Gd2—O21	2.343(6)	Tb2—O21	2.303(4)	Dy2—O21	2.303(9)
Eu2—O27	2.371(4)	Gd2—O22	2.364(6)	Tb2—O22	2.341(5)	Dy2—O22	2.331(9)
Eu2—O22	2.382(5)	Gd2—O27	2.370(5)	Tb2—O27	2.356(4)	Dy2—O27	2.335(8)
Eu2—O17	2.390(4)	Gd2—O17	2.381(6)	Tb2—O17	2.360(4)	Dy2—O16	2.361(8)
Eu2—O16	2.408(4)	Gd2—O16	2.387(6)	Tb2—O16	2.382(4)	Dy2—O17	2.371(8)

Eu2—Cl3	2.656(2)	Gd2—Cl3	2.643(3)	Tb2—Cl3	2.630(2)	Dy2—Cl3	2.618(4)
Eu2—Cl4	2.681(2)	Gd2—Cl4	2.674(3)	Tb2—Cl4	2.655(2)	Dy2—Cl4	2.658(4)

Compound 6		**Compound 7**		**Compound 8**	
Ho1—O13	2.297(2)	Er1—O13	2.293(3)	Yb1—O6	2.251(3)
Ho1—O6	2.304(2)	Er1—O6	2.299(3)	Yb1—O12	2.267(3)
Ho1—O7	2.319(2)	Er1—O7	2.309(3)	Yb1—O7	2.273(3)
Ho1—O2	2.334(2)	Er1—O2	2.326(3)	Yb1—O2	2.280(3)
Ho1—O4	2.339(2)	Er1—O4	2.331(3)	Yb1—O1	2.331(3)
Ho1—Cl2	2.6087(9)	Er1—Cl2	2.5969(13)	Yb1—Cl1	2.6037(11)
Ho1—Cl1	2.6349(9)	Er1—Cl1	2.6214(13)	Yb1—Cl2	2.6149(11)
				Yb2—O21	2.253(3)
				Yb2—O27	2.300(3)
				Yb2—O22	2.301(3)
				Yb2—O17	2.307(3)

				Yb2—O16	2.331(3)
				Yb2—Cl3	2.5750(13)
				Yb2—Cl4	2.6030(13)

Table S2 (cont). Bond lengths [Å] for compounds 2-8

Compound 2		**Compound 3**		**Compound 4**		**Compound 5**	
Ti1—O9	1.738(5)	Ti1—O9	1.740(6)	Ti1—O9	1.752(4)	Ti1—O9	1.735(8)
Ti1—O11	1.791(4)	Ti1—O11	1.787(6)	Ti1—O11	1.788(4)	Ti1—O11	1.788(7)
Ti1—O12	1.933(4)	Ti1—O12	1.942(5)	Ti1—O12	1.939(4)	Ti1—O12	1.934(7)
Ti1—O3	2.074(5)	Ti1—O3	2.073(5)	Ti1—O3	2.068(4)	Ti1—O3	2.072(8)
Ti1—O2	2.094(4)	Ti1—O2	2.082(5)	Ti1—O2	2.080(4)	Ti1—O2	2.076(8)
Ti1—O10	2.191(5)	Ti1—O10	2.195(6)	Ti1—O10	2.198(5)	Ti1—O10	2.184(8)
Ti2—O13	1.751(5)	Ti2—O13	1.762(6)	Ti2—O13	1.760(4)	Ti2—O13	1.743(8)
Ti2—O14	1.780(4)	Ti2—O14	1.788(6)	Ti2—O14	1.784(4)	Ti2—O14	1.779(8)
Ti2—O5	1.939(4)	Ti2—O5	1.937(6)	Ti2—O5	1.952(4)	Ti2—O5	1.934(8)
Ti2—O1	2.050(4)	Ti2—O1	2.047(6)	Ti2—O1	2.047(4)	Ti2—O1	2.046(8)
Ti2—O6	2.133(4)	Ti2—O6	2.129(5)	Ti2—O6	2.123(4)	Ti2—O6	2.156(8)
Ti2—O15	2.172(5)	Ti2—O15	2.179(7)	Ti2—O15	2.175(5)	Ti2—O15	2.182(9)
Ti3—O25	1.739(5)	Ti3—O25	1.755(6)	Ti3—O25	1.748(4)	Ti3—O25	1.747(8)
Ti3—O26	1.777(4)	Ti3—O26	1.785(6)	Ti3—O26	1.786(4)	Ti3—O26	1.780(8)
Ti3—O27	1.940(5)	Ti3—O27	1.948(6)	Ti3—O27	1.947(4)	Ti3—O27	1.964(8)
Ti3—O18	2.081(5)	Ti3—O18	2.083(6)	Ti3—O18	2.078(5)	Ti3—O18	2.067(8)
Ti3—O17	2.093(5)	Ti3—O17	2.096(6)	Ti3—O17	2.087(4)	Ti3—O17	2.078(8)
Ti3—O24	2.192(5)	Ti3—O24	2.179(7)	Ti3—O24	2.190(5)	Ti3—O24	2.187(9)
Ti4—O30	1.777(5)	Ti4—O29	1.779(6)	Ti4—O30	1.787(5)	Ti4—O30	1.775(9)

Ti4—O29	1.783(5)	Ti4—O30	1.782(6)	Ti4—O29	1.788(5)	Ti4—O29	1.786(9)
Ti4—O20	1.926(5)	Ti4—O20	1.912(7)	Ti4—O20	1.929(5)	Ti4—O20	1.939(9)
Ti4—O16	2.056(5)	Ti4—O16	2.059(6)	Ti4—O16	2.054(4)	Ti4—O16	2.059(8)
Ti4—O21	2.135(5)	Ti4—O21	2.131(6)	Ti4—O21	2.146(5)	Ti4—O21	2.128(8)
Ti4—O28	2.176(6)	Ti4—O28	2.176(8)	Ti4—O28	2.186(6)	Ti4—O28	2.169(10)

Compound 6		**Compound 7**		**Compound 8**	
Ti1—O11	1.776(2)	Ti1—O11	1.769(4)	Ti1—O9	1.748(3)
Ti1—O10	1.790(2)	Ti1—O10	1.787(3)	Ti1—O11	1.795(3)
Ti1—O5	1.944(2)	Ti1—O5	1.944(3)	Ti1—O12	1.946(3)
Ti1—O4	2.047(2)	Ti1—O4	2.045(3)	Ti1—O3	2.071(3)
Ti1—O6	2.131(2)	Ti1—O6	2.133(3)	Ti1—O2	2.082(3)
Ti1—O9	2.167(2)	Ti1—O9	2.169(4)	Ti1—O10	2.195(3)
Ti2—O12	1.754(2)	Ti2—O12	1.756(4)	Ti2—O13	1.750(3)
Ti2—O14	1.787(2)	Ti2—O14	1.785(3)	Ti2—O14	1.798(3)
Ti2—O13	1.943(2)	Ti2—O13	1.944(3)	Ti2—O5	1.941(3)
Ti2—O1	2.069(2)	Ti2—O1	2.072(3)	Ti2—O1	2.050(3)
Ti2—O2	2.078(2)	Ti2—O2	2.077(3)	Ti2—O6	2.134(3)
Ti2—O15	2.192(2)	Ti2—O15	2.193(4)	Ti2—O15	2.172(3)
				Ti3—O25	1.747(3)
				Ti3—O26	1.785(3)
				Ti3—O27	1.949(3)
				Ti3—O18	2.079(3)

				Ti3—O17	2.088(3)
				Ti3—O24	2.199(3)
				Ti4—O29	1.790(3)
				Ti4—O30	1.791(3)
				Ti4—O20	1.925(3)
				Ti4—O16	2.044(3)
				Ti4—O21	2.140(3)
				Ti4—O28	2.205(4)